04,08

$CaMoO_4-NaGd(MoO_4)_2$ Solid Solutions: simulation of properties and local structure by the method of interatomic potentials

© V.B. Dudnikova[1], D.I. Antonov[1], E.V. Zharikov[2], N.N. Eremin[1]

[1] Moscow State University,
Moscow, Russia
[2] Prokhorov Institute of General Physics, Russian Academy of Sciences,
Moscow, Russia

E-mail: VDudnikova@hotmail.com

Received June 22, 2022
Revised July 5, 2022
Accepted July 8, 2022

Simulation of $CaMoO_4-NaGd(MoO_4)_2$ solid solutions by the method of interatomic potentials is carried out. It is shown that solid solutions exist in the entire range of compositions and are close to ideal. Dependences on the composition of the lattice parameters and volume of the unit cell, density, bulk modulus, enthalpy, vibrational entropy and heat capacity are obtained. Temperature dependences of heat capacity and vibrational entropy are constructed.

Analysis of the local structure and its changes depending on the composition of the $Ca_{1-x}Na_{x/2}Gd_{x/2}MoO_4$ solid solution showed that in solid solution the interatomic distances of Gd−O are on average 2.62% less, and Na−O is 3.15% greater than the distances of Ca−O. In general, this leads to an increase in the lattice parameters and volume of the unit cell during the formation of $Ca_{1-x}Na_{x/2}Gd_{x/2}MoO_4$ solid solutions compared to $CaMoO_4$.

Keywords: simulation, molybdates, the solid solutions, local structure.

DOI: 10.21883/PSS.2022.11.54195.413

1. Introduction

$CaMoO_4$ (CMO) powellite crystallizes in the scheelite structure (a tetragonal crystal system, space group $(I4_1/a)$) and can be represented by the general formula: ABO_4. The central ion of calcium is coordinated by eight MoO_4-tetrahedra, the point symmetry of the calcium site is S_4.

Powellite-based solid solutions that contain ions of rare earth elements are of interest due to the possibility to use them as phosphor for white LEDs [1]. The possibility of forming solid solutions of powellite with radioactive elements plays an important role in the burial of nuclear waste [2].

The $NaGd(MoO_4)_2$ (NGM) double molybdate also crystallizes in the scheelite structure at statistical distribution of cations in sites of the *A*-sublattice [3–5]. It is of interest as a matrix to create solid-state lasers generating tunable radiation and ultrashort femtosecond pulses in the near IR-range of spectrum [6,7]. In addition, various solid solutions based on sodium-gadolinium molybdate also find applications to create phosphors for white LEDs [8,9].

$CaMoO_4-NaGd(MoO_4)_2$ (CMO−NGM) solid solutions were experimentally investigated in [10–12]. In polycrystalline samples of $NaCaGd(MoO_4)_3$ triple molybdate obtained by the sol-gel method and additionally annealed the Er^{3+} and Yb^{3+} [11] or Ho^{3+} and Yb^{3+} [12] were introduced, that substituted up to 50% of gadolinium ions. In these studies it was found that both nominally pure $NaCaGd(MoO_4)_3$ and substituted samples of triple molybdate had a structure of scheelite.

In [10] the series of polycrystalline samples of $CaMoO_4-NaGd(MoO_4)_2$ solid solutions with different compositions was synthesized where from 10 to 100% of calcium were substituted by gadolinium and sodium. Using the X-ray powder diffraction it was found that even a total substitution of Ca^{2+} with ions of Na^+ and Gd^{3+} does not change the structure of solid solution. It is still identified as a scheelite with random distribution of sodium and gadolinium over calcium positions.

To study the effect of substitution on local structural changes, in [10] the method of time-resolved laser fluorescence spectroscopy (TRLFS) at low temperature ($T < 20$ K) was used. The so-called europium luminescent probe was used, constituting Eu^{3+} ions introduced into samples in an amount of 50 ppm. The study was assumed that the behavior of Eu^{3+} ions fully reflects the behavior of Gd^{3+} ions due to physico-chemical similarity.

Based on results of polarization-dependent TRLFS measurements of $NaGd(MoO_4)_2:Eu$ single crystal sample, the authors of [10] have come to a conclusion that in NGM the point symmetry of the site occupied by a three-valence ion is lowered down to C_{2v} as compared with the initial symmetry of the calcium site in powellite — S_4. According to the authors, the above-mentioned lowering of symmetry is attributable to the displacement of two oxygen atoms in the nearest environment of the cation from the equilibrium state. Unfortunately, the method used does not allow

Table 1. Parameters of interatomic potentials used in the study; O_c — core, O_s — valence shell of the oxygen ion

Interaction	Potential parameters			Atom	Charge, e
	A, eV	λ, Å	c, eV · A^6		
Na−O_S	41894.857	0.193493	0.0	Na	0.85
Ca−O_S	4181.7977	0.264109	0.0	Ca	1.7
Gd−O_S	3558.66	0.2861	0.0	Gd	2.55
Mo−O_S	945.947	0.366617	0.0	Mo	5.1
O_s−O_s	598.8379	0.314838	26.8965	O_c	0.746527
O_s−O_c	$\chi = 56.5628$ eV/Å^2			O_s	−2.446527

determining the local environment of the Na^+ ion in the structure.

The goal of this work is to simulate by the interatomic potential method the $Ca_{1-x}Na_{x/2}Gd_{x/2}MoO_4$ solid solutions, to estimate their structural, physical, and thermodynamic properties, and to analyze the local structure of solid solutions with different compositions.

2. Simulation technique

The simulation was performed by the interatomic potentials method using GULP 4.0.1 (General Utility Lattice Program) software [13], which is based on the procedure of minimization of the energy of interatomic interactions.

The pair potential U_{ij} of the interaction of ions i and j having charges q_i and q_j was determined as follows:

$$U_{ij}(R_{ij}) = q_i q_j e^2/R_{ij} + A_{ij}\exp(-R_{ij}/\rho_{ij}) - C_{ij}/R_{ij}^6, \quad (1)$$

where R_{ij} is the interatomic distance, A_{ij}, ρ_{ij}, C_{ij} are the empirical parameters of the short-range potentials. The range of operation of these parameters in this study was 15 Å for the oxygen-oxygen contact and 10 Å for other contacts. The polarizability of an oxygen ion was accounted by using the „shell model" [14]. The ion core (O_c) of oxygen and its shell (O_s) displaced by a distance of li are coupled by a harmonic elastic constant χ_i:

$$U_i^s = \chi_i l_i^2/2. \quad (2)$$

The calculations were performed in the ion-covalent approximation. Table 1 shows the parameters of the interatomic potentials used in this work. Their values were obtained by optimizing the structural and elastic properties for a number of compounds and were taken from [15,16].

The impact on the simulation results of such factors as approximation character (anisotropic or isotropic), size of a supercell, and solid solution configuration determined by mutual location of the mixed atoms was studied.

As the starting model, scheelite structure $I4_1/a$ with the lattice parameters and atomic coordinates corresponding to $CaMoO_4$ was taken, according to the data of [17]. The simulation was carried out in an anisotropic approximation without any restrictions imposed on atom displacements when the solid solutions were formed and in an isotropic approximation that keeps the crystal structure unchanged. Supercells were used with the sizes of $7 \times 2 \times 2$ and $6 \times 3 \times 2$ of unit cells, that contain 1120 and 1440 particles (atom cores and shells), respectively.

To simulate random distribution of calcium, sodium, and gadolinium ions over A-sites of the supercell, Binar software [18] was used. Configurations were selected with the lowest values of χ^2 that characterize the degree of deviation of component distribution from the statistic distribution. For the isotropic approximation in the $6 \times 3 \times 2$ supercell, for each composition of the solid solution the simulation was carried out for four different configurations with the same minimum value of χ^2, but different in terms of mutual arrangement of cations in the A-sublattice. Properties were estimated using mean values and standard deviations, taking into account all configurations.

The functions of mixing or properties deviation from additivity (ΔA) of $Ca_{1-x}Na_{x/2}Gd_{x/2}MoO_4$ solid solutions were estimated by the difference between the values typical for the solid solution and mechanical mixture of the components, taking into account their molar fraction by the following formula

$$\Delta A = A_{SS} - A_{NGM}x - A_{CMO}(1-x), \quad (3)$$

where A_{SS} — values of these properties for the solid solution; A_{CMO} and A_{NGM} for pure components — $CaMoO_4$ and $NaGd(MoO_4)_2$.

Mixing entropy (ΔS_{mix}) was determined by the sum of configuration (ΔS_c) and vibration (ΔS_{vib}) components. The configuration entropy (S_c) was calculated by the following equation

$$S_c = -kN\Sigma_i c_i \ln c_i, \quad (4)$$

where k — Boltzmann constant, N — Avogadro number, i — number of atom sorts in the substitution site, c_i — atomic fraction of the i-th sort. To obtain values of the

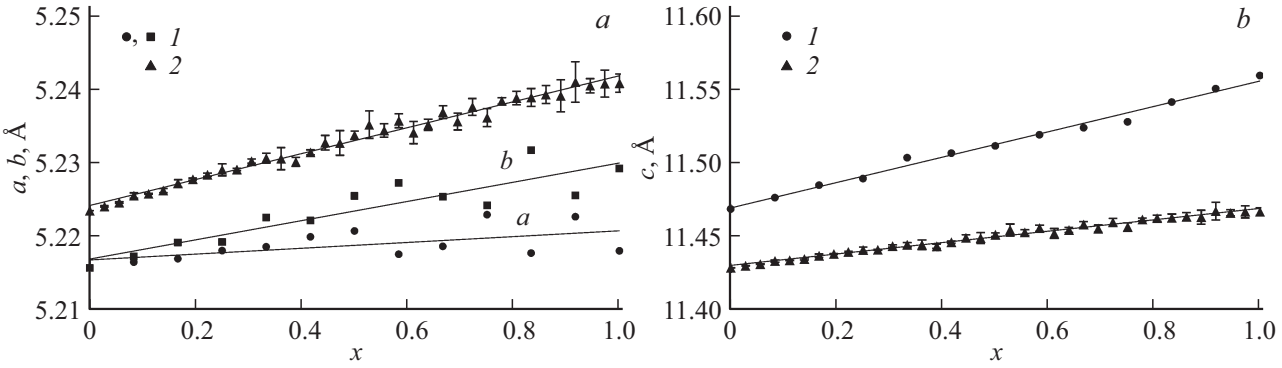

Figure 1. Dependencies of unit cell parameters a, b (a) and c (b) versus composition of $Ca_{1-x}Na_{x/2}Gd_{x/2}MoO_4$ solid solutions in anisotropic approximation (*1*) and averaged over four configurations in isotropic (*2*) approximation.

vibration mixing entropy, vibration spectra of solid solutions and pure components were calculated.

Using GISTOGRAMMA software [18] the numerical data was processed and systematized by bond lengths of Ca–O, Na–O, and Gd–O in the supercell and histograms of bond lengths distribution in the supercell were built-up with a splitting interval of 0.01 Å.

3. Results and discussion

At the preliminary stage of simulation of these solid solutions, the originator of scheelite-like molybdates and the end-member of these solid solutions — $CaMoO_4$ powellite — was simulated. $CaMoO_4$ crystals were simulated in $7 \times 2 \times 2$ and $6 \times 3 \times 2$ supercells. Calculations have shown that the obtained results remain unchanged with the changes in supercell size and match well the experimental structural data [17] taken lattice as a basis for the simulation, as well as the data for parameters and elastic constants obtained earlier in [15]. Thus, for the unit cell we have obtained values of $a = 5.223$ Å and $c = 11.429$ Å in comparison with experimental data of $a = 5.224$ Å and $c = 11.430$ Å [17] and results of [15]: $a = 5.235$ Å and $c = 11.413$ Å, i.e., the differences are not greater than a fraction of percent.

Simulation of $Ca_{1-x}Na_{x/2}Gd_{x/2}MoO_4$ solid solutions in an anisotropic approximation leads to the fact that the structure of solid solutions is slightly different from the initial scheelite structure. In particular, differences between the lattice parameters a and b (Fig. 1, a) and deviations of unit cell angles from 90° arise. The differences between parameters a and b become larger with an increase in x, but do not exceed 0.2–0.3%. An isotropic approximation shell be used to accurately preserve the structure.

Fig. 1 shows the comparison of results obtained for unit cell parameters a, b (a) and c (b) in isotropic and anisotropic approximations for the $6 \times 3 \times 2$ supercell. It can be seen that differences between unit cell parameters calculated in different approximations become larger with an increase in x achieving maximum for NGM the end-member of the series. This is accompanied by the fact that the, values of parameter a for the isotropic approximation are by 0.2–0.4% higher than those for the anisotropic approximation, and values of parameter c are by 0.4–0.8% less.

Comparison of other properties obtained through simulation in isotropic and anisotropic approximations shows that both approximations demonstrate similar character of properties dependence on solution composition. Quantitative differences, like for the parameters of the lattice cell, become larger with an increase in x and achieve maximum for the NGM, which data is provided in Table 2. The small differences as compared with the data of [16], where NGM crystals were simulated, are connected with the impact of configuration or mutual arrangement of cations in the compound. For the isotropic approximation in the $6 \times 3 \times 2$ supercell, errors are specified in Table 2 (in brackets) and in figures, that are resulted from the simulation of four different configurations that differ from each other by mutual arrangement of cations in the *A*-sublattice. It can be seen from Table 2, that estimates of NGM properties when simulated in isotropic and anisotropic approximations in both $7 \times 2 \times 2$ and $6 \times 3 \times 2$ supercells differ from each other insignificantly, in most cases these differences are at a level of a fraction of a percent. And only for the modulus of elasticity maximum differences are 3.4% for the $7 \times 2 \times 2$ supercell and 1.6% for the $6 \times 3 \times 2$ supercell. Also, Table 2 presents the variation range of experimental values of the studied properties according to the data from [19–22] for the NGM crystals grown from stoichiometric composition. The differences connected with the use of different approximations are comparable with the scattering of experimental data or less than it. The difference between properties estimates of $Ca_{1-x}Na_{x/2}Gd_{x/2}MoO_4$ solid solutions simulated in isotropic and anisotropic approximations, in both the $7 \times 2 \times 2$ supercell and in the $6 \times 3 \times 2$ supercell, is less than that for the NGM end-member. Taking into account the experimental data on the scheelite structure of solid solutions, it can be assumed

Table 2. The effect of isotropic and anisotropic approximations, as well as supercell size on properties of the $NaGd(MoO_4)_2$ sodium-gadolinium molybdate, end-member of the series of $Ca_{1-x}Na_{x/2}Gd_{x/2}MoO_4$ solid solutions and comparison with the range of variation of experimental data

Properties	$NaGd(MoO_4)_2$					
	Calculation					Experiment [19-22]
	anisotropic		isotropic			
	$7 \times 2 \times 2$	$6 \times 3 \times 2$	$7 \times 2 \times 2$	$6 \times 3 \times 2$	$7 \times 3 \times 2$ [16]	
a, Å	5.216	5.218	5.244	5.241(1)	5.241	5.221–5.244
b, Å	5.236	5.229	5.244	5.241(1)	5.241	5.221–5.244
c, Å	11.586	11.559	11.474	11.467(3)	11.468	11.412–11.487
V, Å^3	316.368	315.375	315.547	314.9(2)	315.06	311.06–315.89
ρ, g/cm^3	5.250	5.267	5.264	5.274(4)	5.27	5.258–5.339
K, GPa	57.05	61.56	59.11	61(1)	62.46	–
E_{str}, eV	−196.599	−196.645	−196.596	−196.65(3)	−196.67	–
C_V, 300 K J/(mol · K)	113.67	113.66	113.69	113.67(2)	113.66	–
S_{vib}, 300 K J/(mol · K)	126.63	126.27	126.28	126.1(2)	125.93	–

that calculations in the isotropic approximation should be preferable.

As for the effect of supercell size on the simulation results, as a rule, for $Ca_{1-x}Na_{x/2}Gd_{x/2}MoO_4$ solid solutions it is less than that for the end-member $NaGd(MoO_4)_2$, however, the differences change in a non-monotone manner. Differences for solid solutions, as well as in the case of NGM, are not greater than several percents for the modulus of elasticity and tenths or hundredths of percent in other cases.

Thus, properties of solid solutions can be quite adequately described with simulation in supercells of both sizes. However, the calculation of mixing functions in the $7 \times 2 \times 2$ supercell with a little number of compositions and without the estimation of errors related to the deviation of particle distribution in the supercell from the statistical distribution, may give erroneous results. In addition, values for the end-member $NaGd(MoO_4)_2$ are better matched with the results obtained for the larger supercell, i.e., $7 \times 3 \times 2$ [16] (see Table 2). Therefore, the main results are presented for the $6 \times 3 \times 2$ supercell in the isotropic approximation taking into account the error related to the deviation of particle distribution in the supercell from the statistical distribution.

For $Ca_{1-x}Na_{x/2}Gd_{x/2}MoO_4$ solid solutions the estimates were made for the dependencies of lattice parameters (Fig. 1), as well as for the unit cell volume, and for a number of physical and thermodynamic properties in dependence on solid solution composition (Fig. 2). Limits of errors on some dependencies are not distinguishable in the scale of figures.

Approximation of the obtained data made it possible to derive their analytical functions. The change in lattice parameters with changing the composition of the solid solution can be represented by the following equations

$$a = 0.0176x + 5.2241 \quad (R^2 = 0.984), \tag{5}$$

$$c = 0.0386x + 11.4302 \quad (R^2 = 0.984), \tag{6}$$

where R^2 — correlation coefficient. The volume of the unit cell has the following dependence on the composition

$$V = 3.1709x + 311.9389 \quad (R^2 = 0.984). \tag{7}$$

Thus, a little increase in lattice parameters and in the volume of the unit cell takes place in the case of moving from $CaMoO_4$ to NGM. The sum of ion radii of sodium and gadolinium is slightly less than the sum of radii of two substituted cations of calcium: ($r^{3+}_{Gd} = 1.053$ Å, $r^{+}_{Na} = 1.18$ Å, $r^{2+}_{Ca} = 1.12$ Å, CN = 8 [23]). Apparently, the increase in lattice parameters and volume of the unit cell is mainly contributed by the changes in bond lengths connected with emergence of ions in the lattice that add excessive negative (sodium) and excessive positive (gadolinium) charge as compared with the undisturbed structure of $CaMoO_4$.

As the concentration of sodium and gadolinium increases, the density of crystals (Fig. 2, *b*) increases linearly

$$\rho = 1.01x + 4.26 \quad (R^2 = 1). \tag{8}$$

The determining role in this process is played by the increase in concentration of heavy atoms of gadolinium.

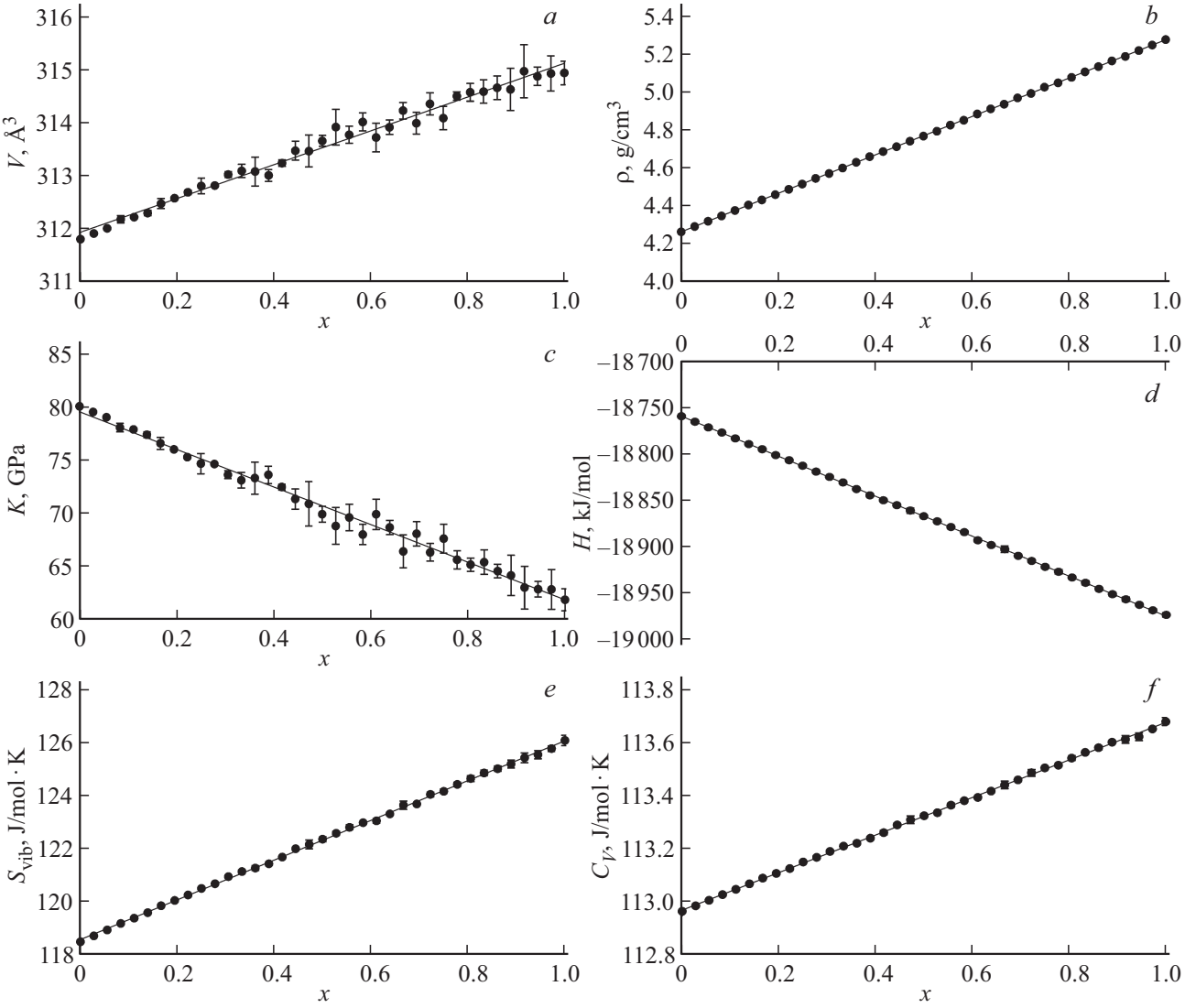

Figure 2. Dependencies of unit cell volume (a), density (b), bulk modulus (c), entalphy (d), as well as vibration entropy (e) and heat capacity at constant volume (f) at 300 K versus the composition of the $Ca_{1-x}Na_{x/2}Gd_{x/2}MoO_4$ solid solution, obtained for the $6 \times 3 \times 2$ supercell.

This effect exceeds the impact of the increase in the volume by substitution of calcium by the lighter sodium.

When moving from $CaMoO_4$ to NGM, the bulk modulus K (Fig. 2, c) and enthalpy H (Fig. 2, d) decrease in accordance with the following equations

$$K = -17.678x + 79.483 \quad (R^2 = 0.986), \tag{9}$$

$$H = -214.23x - 18760 \quad (R^2 = 0.999). \tag{10}$$

Vibration entropy S_{vib} (Fig. 2, e) and heat capacity at constant volume C_V (300 K) (Fig. 2, f) increase

$$S_{vib} = 7.4603x + 118.59 \quad (R^2 = 0.999), \tag{11}$$

$$C_V = 0.7037x + 112.97 \quad (R^2 = 0.999). \tag{12}$$

Calculations have shown that the contribution of vibration entropy to the total entropy of the solid solution is greater than 90%.

Fig. 3, a shows the temperature dependence of heat capacity at constant volume (C_V) for the equimolar solid solution of $Ca_{1-x}Na_{x/2}Gd_{x/2}MoO_4$ obtained in this study. Limits for standard deviations are not shown in the scale of the figure. The differences related to the change in the composition of the solid solution shown in Fig. 2, f are almost indistinguishable in the scale of Fig. 3, a. Therefore, temperature dependencies for end-members of $CaMoO_4$ and NGM solid solutions look like those for the equimolar solid solution. For the comparison with experimental data for temperature dependencies of heat capacity, the calculated values of C_V were converted to values at constant pressure (C_P) using the relationship from [24]:

$$C_P - C_V = 9\alpha^2 KVT, \tag{13}$$

where α — temperature coefficient of linear expansion, K — bulk modulus, V — volume, T — temperature. Data

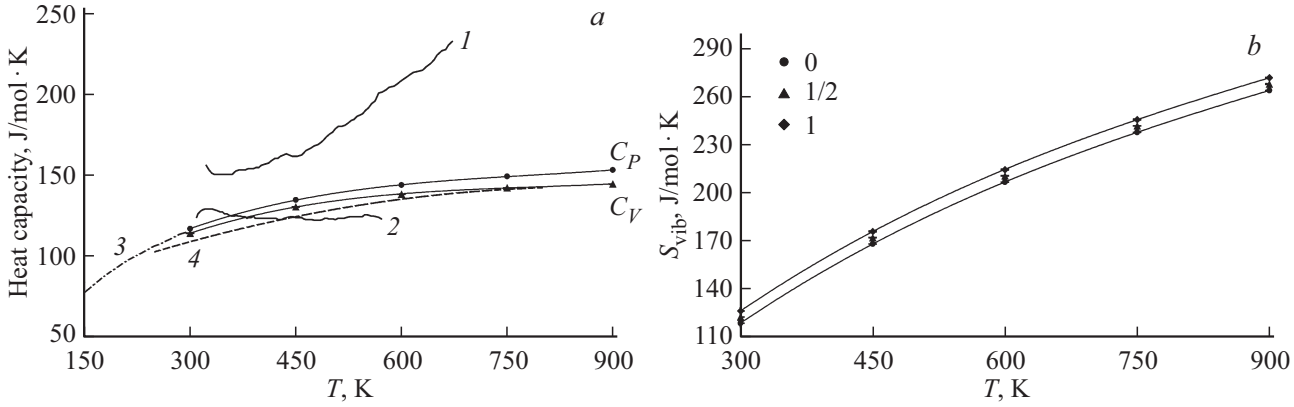

Figure 3. Temperature dependencies of heat capacity at constant volume C_V or pressure C_P (a) and vibration entropy (b) of $CaMoO_4-NaGd(MoO_4)_2$ solid solutions. Also, the heat capacity experimental dependencies $C_P(T)$ are shown for NGM (curves *1* [25] and *2* [26]), $CaMoO_4$ (dot-dashed line *3*) [27] and calculated dependencies $C_V(T)$ for $CaMoO_4$ [28] (dashed line *4*). For the vibration entropy of $Ca_{1-x}Na_{x/2}Gd_{x/2}MoO_4$ solid solutions the data is presented for pure end-members (0 and 1) and for the equimolar composition (1/2).

for C_P is shown in Fig. 3, *a* together with the experimental dependencies $C_P(T)$ for sodium-gadolinium molybdates doped with little quantity of rare earth elements Nd [25] or Tm and Ho [26]: lines 1, 2 according to the data of [25], [26], respectively. It can be seen, that experimental data for NGM are considerably different from each other. The dependencies obtained by us match to a greater extent the results of more recent work [26], curve *2*. Fig. 3, *a* also shows literature data for the temperature dependence of the heat capacity of $CaMoO_4$: experimental dependencies $C_P(T)$ [27] in a temperature range of 150–293 K (dot-dashed line *3*) and simulation results $C_V(T)$ [28] (dashed line *4*). A close match can be seen with our results for solid solutions.

A change in the composition of the solid solution results in some shift of the temperature dependence of vibration entropy. The range of change in the dependencies on the composition of the solid solution is marked in Fig. 3, *b*.

Functions of mixing were studied and Fig. 4 shows some of them. Conspicuous are large errors in the determining of functions of mixing. This is connected with the fact that values of mixing functions, which are relatively small, are determined as a difference between the values that are considerably greater than them by their magnitude.

The study of compositions in addition to those considered earlier in [29], an increase in supercell size, and averaging of values obtained for different configurations made it possible to refine the character of mixing functions for the $Ca_{1-x}Na_{x/2}Gd_{x/2}MoO_4$ solid solution. It can be seen in Fig. 4, that deviation of the mixing functions from additivity is not greater than the errors of calculations related to the simulation of randomly distributed components of *A*-sublattice, from which it follows that the solution of $Ca_{1-x}Na_{x/2}Gd_{x/2}MoO_4$ can be considered as ideal.

Dependencies of the Gibbs free energy on the composition of the solid solution in a temperature range of 300–900 K (Fig. 4, *d*) are indicative of the existence of continuous series of solid solutions $CaMoO_4$–NGM, that matches the experimental data of [10].

The arrays of atom coordinates obtained as a result of calculations were used for the analysis of the local structure of crystals. Fig. 5 shows the nearest environment of a calcium ion in $CaMoO_4$ (5, *a*) and examples of the nearest environment in the solid solution of equimolar composition $Ca_{0.5}Na_{0.25}Gd_{0.25}MoO_4$ for randomly selected sites of ions of calcium (5, *b*), sodium (5, *c*), and gadolinium (5, *d*). It can be seen from the comparison, how the local environment of cations in the *A*-sublattice changes in case of moving from $CaMoO_4$ to CMO–NGM solid solution. All atoms around the central cation undergo shifts from equilibrium states typical for the structure of $CaMoO_4$. Dispersions of interatomic distances (difference between the longest and the shortest distances) increase significantly. At the same time, symmetry of the cation site is lowered down to C_1, in the same manner as it took place in the solid solution of $CaMoO_4-NaEu(MoO_4)_2$ [30]. Based on results of simulation, shifts from equilibrium states are undergone by all oxygen atoms, not only by two of them, and the lowering of symmetry of the *A*-site appears to be greater that reported in [10].

For $Ca_{1-x}Na_{x/2}Gd_{x/2}MoO_4$ solid solutions the histograms were built up for the frequency distribution of interatomic distances (R) in *A*-polyhedra for bonds of Ca–O, Na–O, and Gd–O, the most likely their values and mean values were identified, and dispersion of the distances (ΔR) was estimated.

Fig. 6 shows an example of histograms for the distribution of cation-oxygen bond lengths in *A*-polyhedra for the equimolar composition. These histograms are indicative of the fact that in mean Ca–O bond length in the $Ca_{0.5}Na_{0.25}Gd_{0.25}MoO_4$ solid solution is 2.486(1) Å, while the dispersion of bond lengths is 0.54(5) Å, for Na–O these values are 2.566(2) and 0.60(3) Å, and for Gd–O they are 2.420(1) and 0.47(5) Å respectively. The Na–O bond is

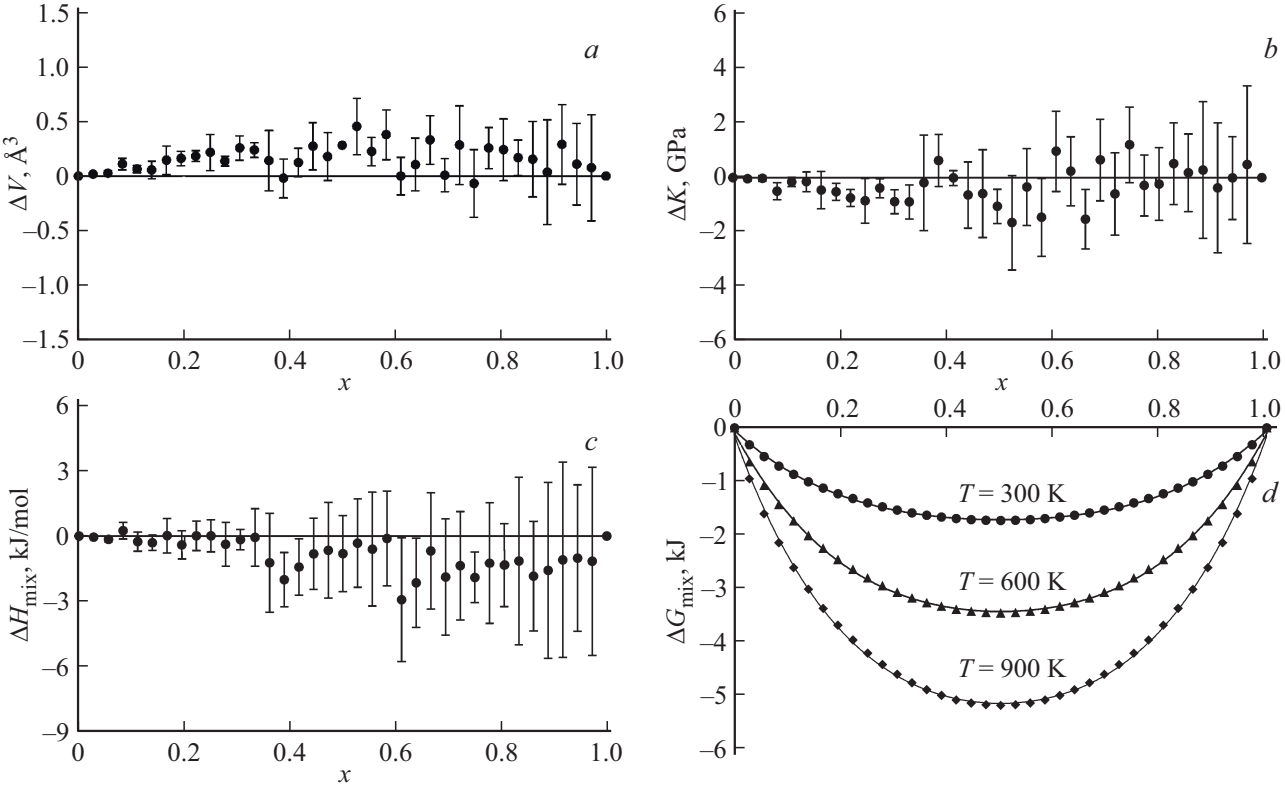

Figure 4. Mixing functions for the unit cell volume (a), modulus (b), bulk and enthalpy (c), Gibbs energy of mixing (d).

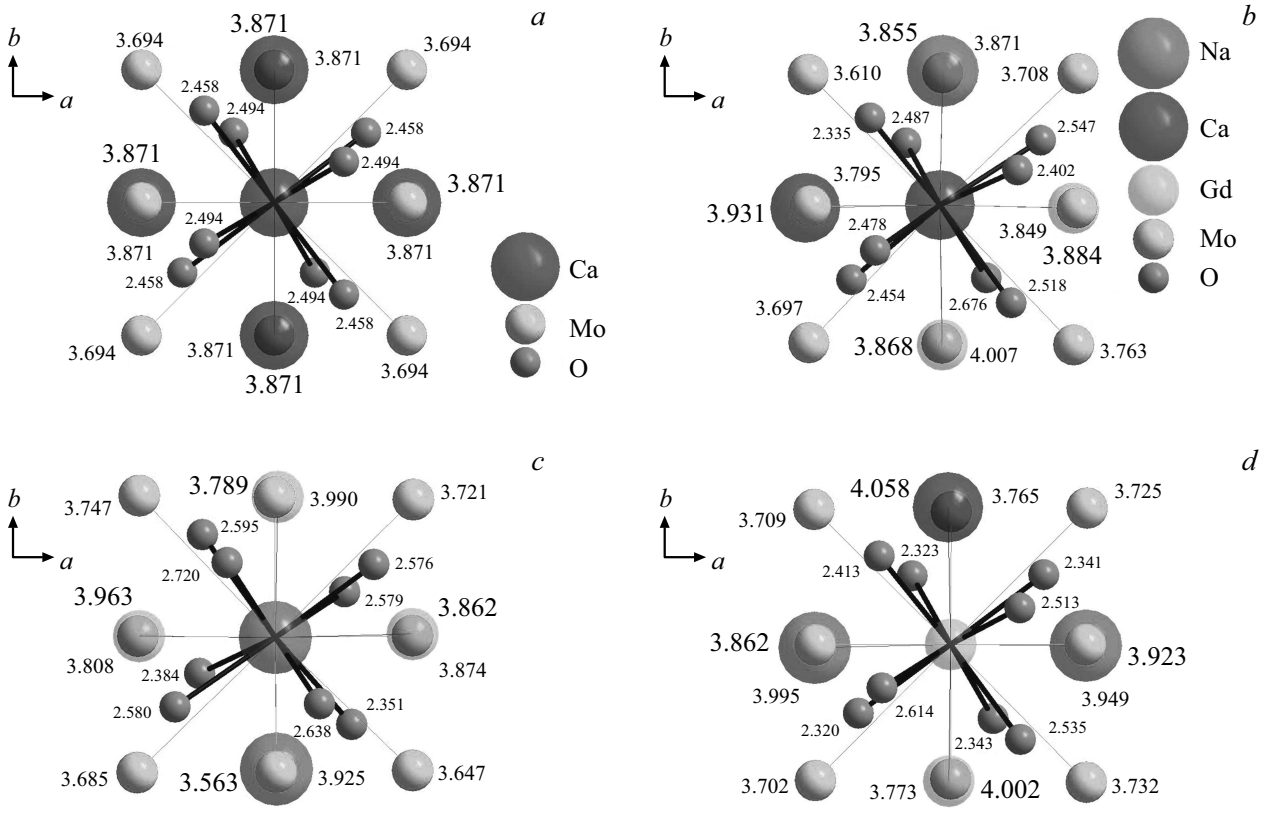

Figure 5. Local environment of calcium ion in $CaMoO_4$ (a), as well as for randomly selected ions of calcium (b), sodium (c), and gadolinium (d) in the $Ca_{0.5}Na_{0.25}Gd_{0.25}MoO_4$ solid solution.

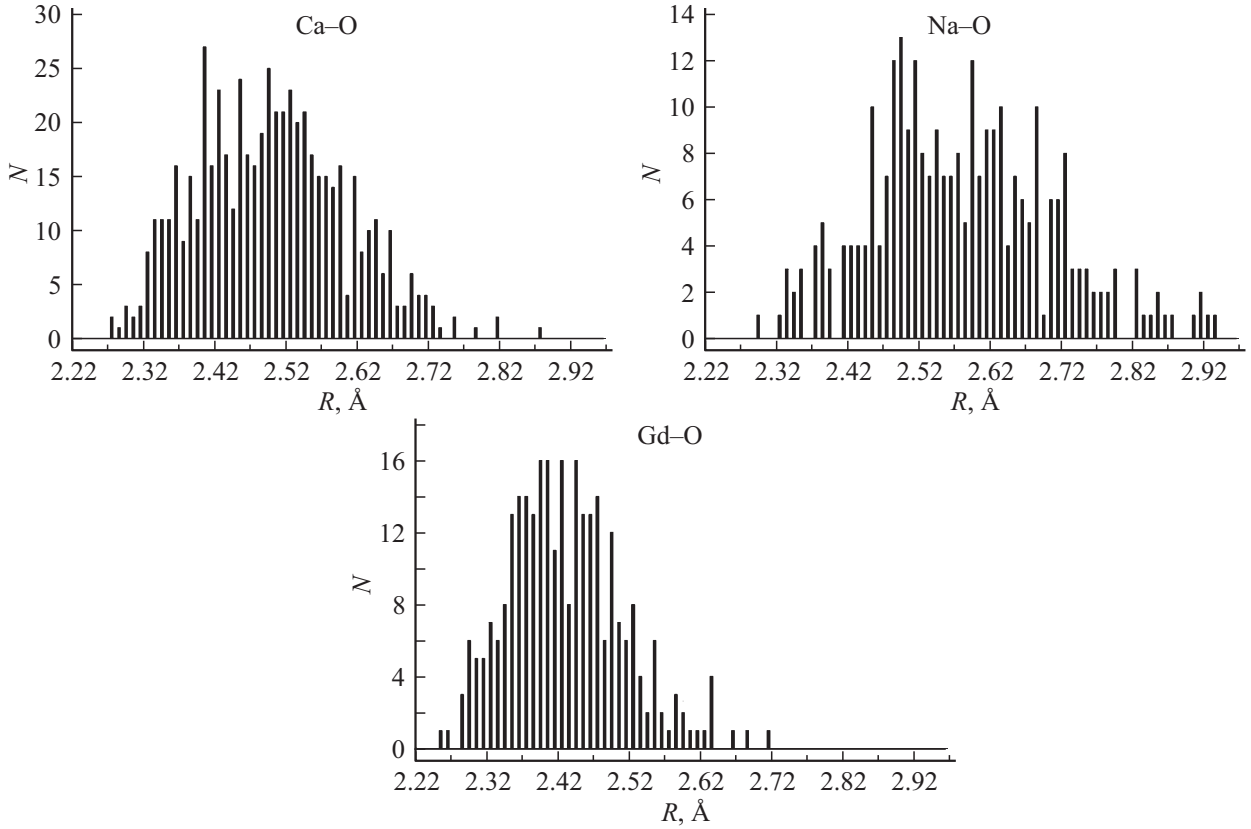

Figure 6. Histograms of bond lengths distribution for Ca−O, Na−O and Gd−O in $Ca_{0.5}Na_{0.25}Gd_{0.25}MoO_4$ solid solution. N — number of bonds with the given interatomic distance.

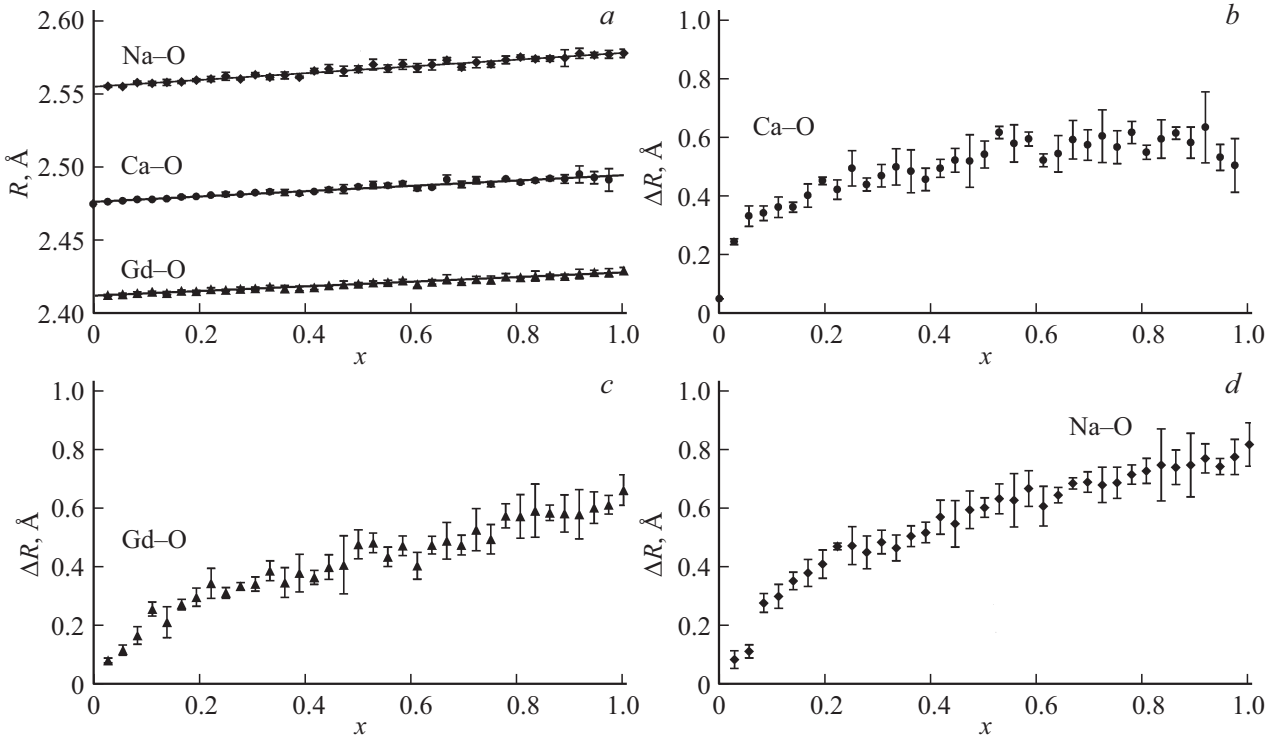

Figure 7. Dependencies of bond lengths of Ca−O, Na−O and Gd−O (a) and their dispersion (b, c, d) on the composition of $Ca_{1-x}Na_{x/2}Gd_{x/2}MoO_4$ solid solution.

characterized by the biggest both mean value and dispersion of the bond length while the Gd−O bond has the lowest values of these parameters.

The results obtained for the entire series of solid solutions are illustrated in Fig. 7, where mean values of Ca−O, Na−O, and Gd−O distances are shown. It is worth noting, that Gd−O distances on average are 2.62% less than Ca−O distances. At the same time, Na−O distances on average are 3.15% greater than Ca−O distances. This results in an increase in lattice parameters and volume of the unit cell when $Ca_{1-x}Na_{x/2}Gd_{x/2}MoO_4$ solid solutions are formed, however, the sum of ion radii of sodium and gadolinium (see above) is slightly less than the sum of radii of two substituted cations of calcium.

As the concentration of Na and Gd in a solid solution increases, mean values of all bond lengths become slightly longer (Fig. 7, *a*), despite the mean ion radius of cations in *A*-polyhedra remains almost unchanged.

At the same time the dispersions of cation-oxygen distances in *A*-polyhedra (ΔR) increase as well. It is interesting to note that the dispersion of rare-earth ion — oxygen interatomic distances in the double molybdate $Na_{0.5}Gd_{0.5}MoO_4$ is higher than that in more complex triple molybdates. The increase in dispersion of Gd−O interatomic distances results in the situation that the crystalline field force acting on gadolinium ions in different polyhedra GdO_8 is slightly different. If this difference is kept in the case of gadolinium substitution by a rare-earth ion of activator, it can cause broadening of activator's spectral lines. Indeed, work [10] reported about experimentally observed broadening of the spectral line ($\lambda \sim 580$ nm) in the excitation spectrum of europium in a NGM crystal (end-member of a series) as compared with solid solutions triple molybdates.

4. Conclusion

$Ca_{1-x}Na_{x/2}Gd_{x/2}MoO_4$ solid solutions were simulated by the method of interatomic potentials. The study covered the impact of such factors as supercell size, character of approximation (anisotropic or isotropic), and configuration of the solid solution on the simulation results. It is shown that lattice parameters unit cell volume, density, vibration entropy, and heat capacity grow with an increase in concentration of sodium and gadolinium that substitute calcium. Bulk modulus and enthalpy decrease. All these dependencies are close to linear ones.

Mixing functions were calculated. It was found that the $Ca_{1-x}Na_{x/2}Gd_{x/2}MoO_4$ solution is close to ideal.

The analysis of the local structure has shown that mean values of Gd−O bond lengths in the solid solution become lower than those of Ca−O, which is connected with the increase in charge and decrease in size of the gadolinium ion as compared with the calcium ion. For sodium, that has lower charge and larger size, mean values of bond lengths increase as compared with the Ca−O bond length. Mean values of Ca−O, Gd−O, and Na−O bond lengths increase linearly in the series of solid solutions in the case of moving from $CaMoO_4$ to $Na_{1/2}Gd_{1/2}MoO_4$, however, these changes are not large. Dispersions of distances in *A*-polyhedra for Ca−O, Na−O, and Gd−O bonds increase as well. It was found that in case of substitution of calcium ions with gadolinium and sodium ions the symmetry of calcium site lowers from S_4 down to C_1.

Conflict of interest

The authors declare that they have no conflict of interest.

References

[1] Y. Hu, W. Zhuang, H. Ye, D. Wang, S. Zhang, X. Huang. J. Alloys Comp. **390**, 226 (2005).
[2] T. Taurines, B. Boizot. J. Am. Ceram. Soc. **95**, 1105 (2012).
[3] A.A. Maier, M.V. Provotorov, V.A. Balashov. Uspekhi khimii **42**, 1788 (1973) (in Russian).
[4] V.K. Trunov, V.A. Efremov, Yu.A. Velikodny. Crystal Chemistry and Properties of Double Molybdates and Tungstates, Nauka, L. (1986). 173 s. (in Russian).
[5] A. Li, J. Li, Z. Chen, Y. Wu, L. Wu, G. Liu, C. Wang, G. Zhang. Mater. Express **5**, 527 (2015).
[6] E.V. Zharikov, C. Zaldo, F. Diaz. MRS Bull. **34**, 271 (2009).
[7] A. Schmidt, S. Rivier, V. Petrov, U. Griebner, X. Han, J. María Cano-Torres, A. García-Cortés, M. D. Serrano, C. Cascales, C. Zaldo. J. Opt. Soc. Am. B **25**, 1341 (2008).
[8] F. Mo, L. Zhou, Q. Pang, F. Gong, Z. Liang. Ceram. Int. **38**, 6289 (2012).
[9] L. Li, D. Dong, J. Zhang, C. Zhang, G. Jia. Mater. Lett. **131**, 298 (2014).
[10] M. Schmidt, S. Heck, D. Bosbach, S. Ganschow, C. Walther, T. Stumpf. Dalton Transact. **42**, 8387 (2013).
[11] C.S. Lim. Infrared Phys.Technol. **76**, 353 (2016).
[12] C.S. Lim, J. Korean Ceram. Soc. **53**, 456 (2016).
[13] J.D. Gale. Z. Kristallograph. **220**, 552 (2005).
[14] B.G. Dick, A.W. Overhauser. Phys. Rev. **112**, 90 (1958).
[15] V.L. Vinograd, D. Bosbach, B. Winkler, J.D. Gale. Phys. Chem. Chem. Phys. **10**, 3509 (2008).
[16] V.B. Dudnikova, E.V. Zharikov. FTT **59**, 841 (2017) (in Russian).
[17] V.B. Aleksandrov, L.V. Gorbaty, V.V. Ilyukhin. Crystallographiya **13**, 512 (1968) (in Russian).
[18] V.S. Urusov, N.N. Eremin. Atomistic Computer Simulation of the Structure and Properties of Inorganic Crystals and Minerals, Their Defects and Solid Solutions, GEOS, M. (2012). 428 s. (in Russian).
[19] M. Schieber, L. Holmes. J. Appl. Phys. **35**, 1004 (1964).
[20] The international database PCPDFWIN. V. 2.02 (1999) JCPDS.
[21] G.M. Kuz'micheva, I.A. Kaurova, V.B. Rybakov, P.A. Eistrikh-Geller, E.V. Zharikov, D.A. Lis, K.A. Subbotin. CrystEngComm **18**, 2921 (2016).
[22] E.V. Zharikov, K.A. Subbotin, A.I. Titov, D.A. Lis, V.V. Voronov, V.G. Senin, V.B. Dudnikova. Cryst. Res. Technol. 1900238 (2020).
[23] R.D. Shannon. Acta Cryst. A **32**, 751 (1976).
[24] C. Kittel Introduction to Solid State Physics. Wiley, NewYork, 1956, Nauka Moscow 1978.

[25] X. Li, Z. Lin, L. Zhang, G. Wang. J. Cryst. Growth **290**, 670 (2006).
[26] C. Wang, H. Yin, A. Li, Y. Wu, S. Zhu, Z. Chen. J. Alloys Comp. **615**, 482 (2014).
[27] M. Morishita, Y. Kinoshita, H. Houshiyama, A. Nozaki, H. Yamamoto J. Chem. Thermodynamics **114**, 30 (2017).
[28] A. Senyshyn, H. Kraus, V. B. Mikhailik, L. Vasylechko, M. Knapp. Phys. Rev. B **73**, 014104 (2006).
[29] V.B. Dudnikova, E.V. Zharikov, D.I. Antonov, N.N. Eremin. In collected book: Problemy kristallologii / Eds. N.N. Eremina. Vyp. 7. KDU, M. (2019). S. 30. (in Russian).
[30] V.B. Dudnikova, E.V. Zharikov, N.N. Eremin. Mater. Today Commun. **23**, 1 (2020).